HHS Public Access

Author manuscript

Anal Chem. Author manuscript; available in PMC 2022 September 16.

Published in final edited form as:

Anal Chem. 2022 June 21; 94(24): 8605–8617. doi:10.1021/acs.analchem.1c05531.

Multiplexed Monitoring of Neurochemicals via Electrografting-Enabled Site-Selective Functionalization of Aptamers on Field-Effect Transistors

Zan Gao[1,†], **Guangfu Wu**[1,†], **Yang Song**[1,†], **Huijie Li**[1], **Yuxuan Zhang**[1], **Michael J. Schneider**[1], **Yingqi Qiang**[1], **Jackson Kaszas**[2], **Zhengyan Weng**[1], **He Sun**[1], **Bryan D. Huey**[2], **Rebecca Y. Lai**[3], **Yi Zhang**[1,*]

[1]Department of Biomedical Engineering and the Institute of Materials Science, University of Connecticut, Storrs, CT 06269, USA.

[2]Department of Materials Science and Engineering and the Institute of Materials Science, University of Connecticut, Storrs, CT 06269, USA.

[3]Department of Chemistry, University of Nebraska-Lincoln, Lincoln, NE 68588, USA.

Abstract

Neurochemicals corelease has received much attention in understanding brain activity and cognition. Despite many attempts, the multiplexed monitoring of coreleased neurochemicals with spatiotemporal precision and minimal crosstalk using existing methods remains challenging. Here, we report a soft neural probe for multiplexed neurochemical monitoring via electrografting-assisted site-selective functionalization of aptamers on graphene field-effect transistors (G-FETs). The neural probes possess excellent flexibility, ultralight mass (28 mg), and a nearly cellular-scale dimension of 50 μm × 50 μm for each G-FET. As a demonstration, we show that G-FETs with electrochemically grafted molecular linkers (-COOH or -NH_2) and specific aptamers can be used to monitor serotonin and dopamine with high sensitivity (limit of detection: 10 pM) and selectivity

*Corresponding author: yi.5.zhang@uconn.edu.
†These authors contributed equally.

Author Contributions

ZG, GW, and YS contributed equally to this work. ZG, GW, and YZ conceived of the idea and designed the experiments; GW, HL, and YQ designed and fabricated graphene-field effect transistors; ZG, YS, YZ, ZW, and HS contributed to the electrografting, functionalization, and characterizations; JK and BDH performed the AFM measurement; MS collected the mice brain tissue for *ex vivo* studies. RL provided guidance regarding the site-selective functionalization via electrografting; ZG, GW, YS, and YZ analyzed the data and wrote the manuscript. All authors discussed the results and contributed to the final manuscript.

Additional information

Supplementary Information

Competing financial interests: The authors declare that they have no competing interests.

Supporting Information available: All data needed to evaluate the conclusions in the paper are present in the paper and/or the Supplementary Materials: Schematic illustration of the preparation of contact pads (source-drain) on the polyimide (PI) substrate and transferring graphene to the contact pads (Figures S1); CV curves of G-FET before and after the electrografting with carboxyl group (Figure S2) and amino group (Figure S3); Transfer characteristics of a G-FET serotonin sensor exposed to dopamine and dopamine sensor exposed to serotonin (Figure S4); Change of the voltage at Dirac point (V_{dp}) of dopamine and serotonin sensors after incubating in rat CSF solution at room temperature for 24, 48, 72, and 96 hours (Figure S5); *Ex vivo* studies of dopamine sensors in harvested mouse's brain tissue (Figure S6); *Ex vivo* studies of serotonin sensors in harvested mouse's brain tissue (Figure S7); *In vitro* studies using brain tissue phantom models (Figure S8); Responses of serotonin and dopamine sensors when exposing a multiplex neural probe into various serotonin concentrations (Table S1); Responses of dopamine and serotonin sensors when exposing a multiplex neural probe into various dopamine concentrations (Table S2).

(dopamine sensor > 22-fold over norepinephrine; serotonin sensor > 17-fold over dopamine). In addition, we demonstrate the feasibility of the simultaneous monitoring of dopamine and serotonin in a single neural probe with minimal crosstalk and interferences in phosphate-buffered saline, artificial cerebrospinal fluid, and harvested mouse brain tissues. The stability studies show that multiplexed neural probes maintain the capability for simultaneously monitoring dopamine and serotonin with minimal crosstalk after incubating in rat cerebrospinal fluid for 96 hours, though a reduced sensor response at high concentrations is observed. *Ex vivo* studies in harvested mice brains suggest the potential applications in monitoring the evoked release of dopamine and serotonin. The developed multiplexed detection methodology can also be adapted for monitoring other neurochemicals, such as amino acids and neuropeptides, by simply replacing the aptamers functionalized on the G-FETs.

Graphical Abstract

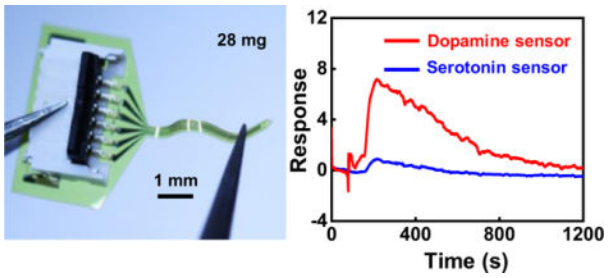

Keywords

soft neural probes; multiplexed neurochemical monitoring; electrochemical grafting; dopamine and serotonin

Introduction

Complex behaviors, such as cognition, perception, and action, are conducted through dynamic neural networks of the brain, which are subject to the transmission of neurochemicals[1, 2]. More than two hundred neurochemicals have been identified in the brain, including monoamines (dopamine (DA), serotonin), peptides, amino acids, lipids, and other small molecules (e.g., acetylcholine)[3, 4]. The abnormal level of certain types of neurochemicals is related to various neuropsychiatric and neurological disorders, such as Parkinson's disease[5–10], schizophrenia[11], and Alzheimer's disease[12]. Many studies have demonstrated the corelease of multiple neurochemicals from neurons[13–15]. For example, increasing evidence has shown that subpopulations of ventral tegmental area (VTA) neurons are capable of releasing dopamine (DA) and gamma-aminobutyric acid (GABA), or DA and glutamate, simultaneously[16, 17]. These diverse signaling mechanisms are implicated in the creation of thinking and impulse signals that are directly related to various behaviors and disorders[18, 19]. However, our understanding of these multiple neurochemicals-involved neurotransmission mechanisms is very limited. This is, in part, because current measurement technologies have limited spatial/temporal precision and molecular specificity for multiplexed neurochemicals identification and detection.

In past decades, with the advances in neuroscience and micro/nanofabrication, groundbreaking sensors have been developed to target specific brain regions at different scales[20–22]. The main techniques for neurotransmitter monitoring include the following several types: 1) nuclear medicine tomographic imaging, such as positron emission tomography (PET)[23]; 2) optical sensing techniques, such as surface-enhanced Raman spectroscopy (SERS)[24, 25], fluorescence[26, 27], chemiluminescence[28], optical fiber biosensing[29] and colorimetry[30]; 3) electrochemical methods[31–33], like fast-scan cyclic voltammetry (FSCV)[34–36] and amperometry[37]; 4) mass spectrometry[25, 38, 39]; and 5) microdialysis sampling (typically coupled with mass spectrometry analysis)[40–44]. While each of these techniques has its pros and cons[4, 45, 46], it is still a significant challenge to build a system that can effectively capture the transient dynamics of neurotransmitters with a high temporal resolution, cellular scale spatial resolution, superior sensitivity, and selectivity, not to mention empowering the tools with multiplexed monitoring capabilities. Among these methods, FSCV, microdialysis, and genetically encoded fluorescent sensors are three widely used or emerging techniques for neurotransmitter monitoring[47]. Specifically, FSCV possesses better temporal resolution (milliseconds) and sensitivity (nanomolar). Because of that, coupling FSCV with voltammogram analysis (multivariate penalized regression, partial least squares regression, and deep learning) has been used to distinguish voltammograms from multiple neurochemicals, thereby making it possible for multiplexed analysis[32, 48, 49]. FSCV, however, fails to distinguish some structurally similar neurotransmitters, such as dopamine and norepinephrine[50–52]. Microdialysis suffers from the large temporal resolution (typically several minutes) and low spatial resolution because of the semipermeable membrane and large probe size (150–440 μm in diameter)[53, 54]. Recently, genetically encoded fluorescent sensors have been developed to image the dynamics of neurochemical release *in vivo*, including DA and glutamate[20, 55–57]. However, the multiplex monitoring with high selectivity and non-overlapping spectra beyond dual-color imaging of glutamate and DA is challenging[47]. Additionally, the complicated genetic modification process and the requirements of coupling with fiber photometry for neural chemical monitoring limit the practical applications of these genetically encoded sensors[57].

A previous study reported an aptamer-modified In_2O_3 field-effect transistor (FET) biosensors for small molecule detection, including serotonin, dopamine, glucose, and sphingosine-1-phosphate under high-ionic strength conditions[58]. However, the large device size, bulky, and rigid component materials lead to constrained spatial resolution and potential brain tissue damage, limiting its practical application in a chronic study. Most recently, implantable aptamer-modified field-effect transistors were reported for monitoring serotonin or dopamine *in vivo*[59, 60]. Although these studies represent significant progress for individual neurotransmitter monitoring, like dopamine or serotonin, it is still challenging to achieve simultaneous monitoring of different types of neurochemicals with spatiotemporal precision and molecular specificity.

Here, we report a soft neural probe for multiplexed neurochemical sensing via electrografting-enabled site-selective functionalization of aptamers on G-FETs. We show that the developed G-FET sensors selectively functionalized with specific aptamers can be used to simultaneously monitor two important neural neurochemicals (serotonin and dopamine) with high sensitivity, selectivity, and minimal mutual interferences. Such a

spatially controlled electrochemical functionalization method could potentially empower the G-FET arrays with an increased number of sensing channels for multiplexed neurochemical monitoring, such as dopamine, serotonin, norepinephrine, and neuropeptides, suggesting the broad applications in neuroscience research.

Results and Discussion

Design, fabrication, and functionalization of G-FETs for multiplexed neurochemical monitoring

As illustrated in Figures 1A and B, we designed a filament neural probe (~400 μm wide, ~8.4 μm thick, 6.2 mm long), consisting of two side-by-side G-FET sensors selectively functionalized with two different types of aptamers and encapsulated with a thin layer of SU-8. The source and drain contact pads (15 nm chromium and 90 nm gold) of G-FET were patterned on a thin-film polyimide (PI, 7.6 μm thick) through the photolithography, metal deposition, and lift-off processes (Figure S1A). After that, the chemical vapor deposition (CVD)-grown graphene on copper foil was transferred, patterned, and assembled with the fabricated source and drain electrodes to make the G-FETs (Figure S1B). Finally, the soft G-FET was encapsulated with a lithography-defined thin layer of SU-8 (~ 0.8 μm thick). Figures 1B and 1C show the optical and SEM images of the fabricated neural probe. The neural probe possesses excellent flexibility and ultralight mass (28 mg) with a nearly cellular-scale dimension of 50 μm × 50 μm for each G-FET, which is much smaller than that of microdialysis probes (150–440 μm in diameter). The ultralow bending stiffness (~7.9×10^{-11} N·m^2, a value six orders of magnitude smaller than that of commonly used neural probes, such as a 230-μm outer diameter optical fiber[61]) and lightweight construction allow the implantation of the probe into the deep brain area with reduced tissue damage, inflammation, and motion artifact[62–64].

The cleanliness of the graphene surface strongly affects the electronic properties of graphene and the final sensing capabilities of G-FETs. Here, a simple bubble-free electrochemical (EC) treatment was used to rapidly clean the residual polymethyl methacrylate (PMMA) on the graphene surface after the wet transfer process[65]. During the EC treatment, the G-FET was used as the working electrode, Ag/AgCl as the reference electrode, and Pt as the counter electrode, respectively. More specifically, cyclic voltammetry (CV) scans at a scan rate of 0.5 V s^{-1} (−0.7 V to 0 V) were performed to remove the residual negatively charged PMMA polymer, de-dope the graphene surface, and recover its intrinsic electrical properties. The cleaned graphene surface was further modified with a functional group and functionalized with a specific type of aptamer for neurotransmitter monitoring.

The graphene surfaces of the two side-by-side G-FETs were selectively functionalized with COOH and -NH_2 groups, respectively, through electrochemical-grafting methods. The electrografted -COOH and -NH_2 groups serve as linkers to anchor two aptamers with different functionals groups through the 1-ethyl-3-(3-dimethylaminopropyl) carbodiimide (EDC)/N-hydroxysuccinimide (NHS) reaction (serotonin aptamer: 5′-AmC6-CGA CTG GTA GGC AGA TAG GGG AAG CTG ATT CGA TGC GTG GGT CG-3′; dopamine aptamer: 5′/COOH/CGA CGC CAG TTT GAA GGT TCG TTC GCA GGT GTG GAG TGA CGT CG-3′) for the detection of serotonin and dopamine, simultaneously. Typically,

the aptamers are attached to the graphene surface through a pyrene-based π-π stacking[66, 67]. Although G-FET functionalized with π-π stacking usually has better sensitivity as it doesn't change the structure of graphene, the weak bonding between aptamer and graphene may make it not ideal for *in vivo* applications. Different from the widely used noncovalent π-π stacking to anchor aptamer on graphene surface[67, 68], in this study, the EDC/NHS reaction enabled the formation of a covalent bond between the graphene surface and aptamers[69, 70], which is critical to achieve long-term stability of the designed neural probe in the chronic *in vivo* study.

G-FETs modified with target-specific recognition components could directly enable bio-detection in physiological conditions[68]. However, the shielding effect of the electrical double layer, characterized as Debye screening length[71], prevents biosensing. Meanwhile, the small target molecules with few or no charges could not trigger enough transconductance change of G-FET, leading to minimal response. Recent studies showed that aptamers, selected through SELEX[72], could overcome these limitations for small molecular detection[58]. When small molecular targets, like dopamine and serotonin, bind with the target-specific aptamer, it will cause the conformational change of the anchored aptamers on graphene[58, 73], changing the doping state of graphene, and leading to a measurable source-drain current change of the G-FETs (Figure 1D). The change in source-drain current of G-FETs can be correlated with the concentration of dopamine or serotonin (Figure 1D).

Eletrografting of -COOH group and functionalization of serotonin aptamer on G-FET

The strategy for developing the serotonin aptamer functionalized G-FET sensor is illustrated in Figure 2A. Briefly, an aqueous solution of $NaNO_2$ was dropwise added to p-aminobenzoic acid (p-ABA) (1 M HCl) to form a homogeneous mixture. The mixed solution was then kept in the ice/water bath to form the diazonium salt (ClN_2^+-Ph-COOH). The selected G-FET array was then immersed into the above solution and used as a working electrode to link the -Ph–COOH on the graphene surface by applying CV scans from −0.6 V to 0.5 V for 5 cycles (scan rate = 100 mV s^{-1}). During the first cycle, a reduction peak appeared at −0.4 V, which disappeared during the subsequent cycles and the CV curves gradually became stable after the second scan, indicating the electrochemical reduction of ClN_2^+-Ph-COOH to form the modified graphene-Ph-COOH surface[74] (Figure 2B). The surface functionalization of graphene with -Ph-COOH can be further evidenced by the Raman (Figure 2C) and atomic force microscopy (AFM, Figure 2D) tests. The Raman spectra of graphene on G-FET before and after electrochemical grafting are shown in Figure 2C. There are two prominent peaks for the bare graphene, a single symmetric 2D band at 2700 cm^{-1} and a G band at 1580 cm^{-1}. The intensity ratio between the 2D band and the G band is around 2.22, which is a typical characteristic of monolayer graphene, indicating that the transferred graphene on G-FET remains high quality after the transferring process[75]. Furthermore, after the electrografting process, there is a new D band appears at ~1350 cm^{-1}, which usually represents the defects and disordered graphite structures[76]. The appearance of the D band indicates the success of the electrochemical grafting reaction, which broke the sp^2 bond of graphene and linked the -Ph-COOH on graphene through the diazonium reaction. The ratio of I_{2D}/I_G, after electrografting of COOH group, is 1.47, indicating the binding of the functional -COOH group on the graphene surface.

A clear surface morphology change of graphene can be observed from the AFM image after the electrochemical grafting process. As shown in Figure 2D, compared to the pure graphene surface, a much rougher surface with small nanoparticles can be observed from the AFM image of the electrografted graphene surface. The significant surface morphology change could be attributed to the electrografting formation of -Ph-COOH on graphene. The electrografting was further highlighted by the cyclic voltammetric characterization of the graphene surface before and after the electrografting (Figure S2). After electrografting, the anodic current of $Fe(CN)_6^{4-}$ to $Fe(CN)_6^{3-}$ significantly reduced, suggesting the barriers on the graphene surface to the electron transfer. The grafted -Ph-COOH on graphene serves as a linker to functionalize serotonin aptamer with $-NH_2$ group through an EDC/NHS reaction.

Figure 2E shows the transfer curves of the fabricated G-FETs after electrochemical cleaning, electrografting, and aptamer functionalization. Clearly, after the electrochemical cleaning process, there is an upper and left shift of the V-shaped transfer curve. The slightly increased current response and left shift of the Dirac point suggested that the electrochemical cleaning increased the conductivity and changed the doping state of the graphene[66, 68]. The down and right shift of the transfer curve after the electrografting of the -COOH group further proves the successful diazonium reaction, which broke the sp^2 bond of graphene and introduced the -Ph-COOH group, leading to the increased resistance and reduced current response. After the serotonin aptamer functionalization with EDC/NHS reaction, we can see a slight down and left shift of the transfer curve mainly due to the non-electrostatic stacking interactions between aptamer and graphene or donor effect[68].

To quantify the sensing performance of the functionalized G-FET serotonin sensor, the functionalized G-FETs linked with serotonin aptamers were exposed to the target solution with various concentrations to record the source-drain current (I_{ds}). The electrical response is defined as $\Delta I_{ds}/I_0 \times 100\%$, where ΔI_{ds} is the source-drain current change caused by the addition of serotonin and I_0 is the initial signal without the addition of serotonin. During the measurement, the gate voltage V_G was fixed at 0 mV to avoid possible chemical reactions such as water electrolysis, dielectric layer breakdown, and the denaturing of the recognition components. As seen in Figure 2F, the electrical response decreases as the increase of serotonin concentration ranging from 10 pM to 100 μM in phosphate-buffered saline) (1× PBS, pH 7.4), which covers the physiologically relevant serotonin concentration in cerebrospinal fluid (CSF)[45, 77]. The serotonin sensor achieves a limit of detection (LOD) as low as 10 pM. To investigate the molecular specificity of the functionalized G-FET serotonin sensor, the electrical response of the serotonin sensor was monitored when exposed to other neurochemicals, which had concentrations three orders of magnitude higher than that of serotonin, including dopamine, norepinephrine, and gamma-aminobutyric acid (Figure 2G). Compared to the response when exposed to 100 μM dopamine, norepinephrine and gamma-aminobutyric acid, the serotonin sensor showed at least 17 times higher response when exposed to 100 nM serotonin, indicating its high selectivity for serotonin monitoring.

Eletrografting of $-NH_2$ group and functionalization of dopamine aptamer on G-FET

The -Ph-NH_2 group was electrografted on the graphene surface through the diazonium reaction (Figure 3A). Briefly, the selected G-FET pattern was used as a working electrode

and then immersed into the prepared diazonium salt (ClN_2+-Ph-NH_2) solution to link the -Ph-NH_2 on the graphene surface by using CV scans for 5 cycles from −0.6 V to 0.5 V (scan rate = 100 mV s^{-1}).

After the first cycle, the reduction peak at −0.2 V disappeared, while stable CV curves formed after the second cycle, indicating the electrochemical reduction of ClN_2^+-Ph-NH_2 to -Ph-NH_2 on the graphene surface (Figure 3B). From the Raman spectrum (Figure 3C), we observed a high intensity of the D band, and an I_{2D}/I_G ratio of 1.32, indicating a covalent functionalization of the graphene surface after the electrografting. AFM images demonstrated the formation of rough structures on the graphene surface after the electrografting process, which provides additional evidence to show the success of the diazonium reaction (Figure 3D). The electrografting of -NH_2 group was further supported by the CV scan of G-FET (electrolyte containing 1 mM $Fe(CN)_6^{3-}$ and 0.10 M KNO_3) in which a significantly reduced anodic current was observed after the electrografting process (Figure S3).

The transfer curves of the bare G-FET, cleaned G-FET, and G-FET with electrografting (-NH_2 group) and dopamine aptamer functionalization are shown in Figure 3E. A reduction of source-drain current and p-doping effect were observed after the electrografting process, mainly due to the diazonium reaction, which broke the sp^2 bond of graphene and introduced the -Ph-NH_2 group. Like the serotonin aptamer, surface functionalization with the dopamine aptamer caused a left shift of the transfer curves. To study the sensing performance of the G-FET dopamine sensor, G-FETs functionalized with dopamine aptamers were exposed to the target solution with various concentrations. As seen in Figure 3F, the electrical response increases with the increase of physiologically relevant dopamine concentration ranging from 1 nM to 100 μM in 1× PBS. Signal drifts were observed in Figure 3F, which could be attributed to imperfect binding and the resulting rearrangement of aptamer structures and to the nonspecific adsorption on the graphene surface. It has been known that FSCV lacks the molecular specificity to distinguish dopamine from norepinephrine due to the overlap of voltammetric patterns[45, 78]. To investigate whether the G-FET dopamine sensors could distinguish dopamine from norepinephrine and other neurochemicals, the electrical response of the dopamine sensor was recorded when exposed to other neurochemicals that had concentrations three orders of magnitude higher than that of dopamine (Figure 3G). Compared to the electrical responses toward the detection of 100 μM norepinephrine, serotonin, and gamma-aminobutyric acid solution, the dopamine sensor showed 22 times higher response toward the detection of 100 nM dopamine, indicating a high molecular specificity of the dopamine sensors.

Electrografting-enabled site-selective functionalization of both serotonin and dopamine aptamers on G-FETs for multiplexed neurochemical monitoring

To enable simultaneous monitoring of dopamine and serotonin in a single neural probe, the graphene surfaces of two G-FETs were sequentially functionalized with -COOH and -NH_2 through the electrografting method (Figure 4A). After that, through the EDC/NHS reaction, serotonin aptamer with -NH_2 group and dopamine aptamer with -COOH group were able to selectively link on the graphene surfaces functionalized with -COOH and

-NH_2, respectively. Figure 4A illustrates the electrografting and functionalization process of G-FETs for multiplexed neural probe design. One of the major challenges for multiplexed detection in a single neural probe is the crosstalk and interferences between two sensors. Here, to study the possible interferences between the dopamine and serotonin sensors, we simultaneously measured the electrical response of dopamine and serotonin sensors toward the detection of dopamine and serotonin ranging from 10 pM to 100 μM (Figures 4B and C). The response of the serotonin sensor decreased with the increase of serotonin concentration ranging from 10 pM to 100 μM in 1× PBS. In contrast, the response of the dopamine sensor only slightly increased (~1.1%) towards the detection of interfering serotonin with a concentration up to 100 μM (Figure 4B and Table S1). Figure 4C shows the real-time response of dopamine and serotonin sensors when exposing the multiplexed neural probe to various dopamine concentrations ranging from 10 pM to 100 μM in 1× PBS. Like serotonin sensors, the dopamine sensors achieve a LOD of 10 pM. A minimal sensor response (~0.6%) was observed when exposing the serotonin sensor to interfering dopamine with a concentration up to 100 μM (Figure 4C and Table S2). The minimal crosstalk and interference are further highlighted by measuring the transfer characteristics of G-FET serotonin sensors exposed to dopamine and G-FET dopamine sensors exposed to serotonin (Figure S4). Overall, these studies demonstrate the feasibility of multiplexed monitoring of dopamine and serotonin in a single neural probe with small crosstalk and interferences, suggesting its potential to study the corelease of multiple neurochemicals in broad neuroscience applications.

In this study, we observed a decrease in electrical response (V_G=0 V) with the increase of serotonin concentration mainly due to the conformational change of aptamer in the presence of serotonin bringing the aptamer away from the graphene channel[58], leading to a decrease of transconductance and n-doping effect on graphene surface (Figure 4D). Different from the serotonin aptamer, the presence of dopamine causes an increase in the source-drain current of G-FET dopamine sensor (V_G=0 V), mainly due to the conformation change of dopamine aptamer, bringing it closer to the G-FET surface[58], leading to a p-doping effect on G-FET (Figure 4E).

Multiplexed monitoring in aCSF with BSA

To evaluate the sensing performance of aptamer functionalized multiplexed neural probes in a more complex environment, we exposed the dopamine and serotonin sensors to solutions with various concentrations of dopamine or serotonin in aCSF with proteins [1 mg/mL bovine serum albumin (BSA), 13 mM glucose, 125 mM NaCl, 3 mM KCl, 2.5 mM $CaCl_2$, 1.3 mM $MgSO_4$, 1.25 mM NaH_2PO_4, and 26 mM $NaHCO_3$]. BSA, as a commonly used protein, was chosen to mimic the protein-rich brain microenvironment[79]. As shown in Figures 5A and B, the electrical response increases/decreases with the increase of the physiologically relevant concentration range of dopamine or serotonin from 10 pM to 100 μM. In addition, no significant differences were observed in the sensor response with the addition of 1 mg/mL BSA in aCSF (Figures 5C and D), demonstrating the potential applications of multiplexed neural probes in protein-rich brain microenvironments.

The stability of multiplexed neural probes in rat CSF

Furthermore, we studied the stability of aptamer functionalized G-FET dopamine and serotonin sensors in rat CSF (BioIVT Elevating Science). The study started with monitoring the transfer curve of aptamer functionalized G-FETs before and after incubating in rat CSF at room temperature for 24, 48, 72, and 96 hours. It is not surprising that a significant left and downshift of transfer curves are observed after incubating the device in rat CSF for 24 hours (Figures 6A and S5), probably due to the non-specific adsorption of proteins in rat CSF on the sensor surface. We then wondered whether this leftward downshift of transfer curves influenced the capability of multiplexed neural probes to monitor dopamine and serotonin. To answer this question, after incubating in rat CSF at room temperature for 96 hours, we used multiplexed neural probes to monitor different concentrations of dopamine ranging from 1 nM to 10 μM in aCSF. As shown in Figure 6B, the electrical responses of dopamine sensors increase with the increase of the physiologically relevant concentration range of dopamine from 1 nM to 10 μM. In contrast, a minimal sensor response was observed for serotonin sensors (Figure 6B). Compared with the electrical responses of as-prepared multiplexed neural probes, the incubation with rat CSF for 96 hours causes a reduction of sensor signals at higher concentrations (100 nM and 10 μM) (Figure 6C), probably due to the non-specific adsorption of various proteins in the complex rat CSF on the sensor surface that could block the available aptamers to capture the dopamine. Inspired by these stability studies of monitoring dopamine, we also studied the stability of multiplexed neural probes for monitoring serotonin by incubating the probe in rat CSF at room temperature for 24, 48, 72, and 96 hours (Figures 6D, E, and F). Like dopamine sensors, we observed a left and downshift of transfer curves (Figure 6D), as well as a reduction of sensor response for monitoring higher concentrations of serotonin (10 nM and 100 nM) (Figure 6F). Nevertheless, the multiplexed neural probe retained the capability of monitoring serotonin ranging from 1 nM to 100 nM in aCSF with minimal crosstalk (Figure 6E). Overall, these studies showed that multiplexed neural probes maintain the ability to simultaneously monitor dopamine and serotonin with minimal crosstalk after incubating in rat CSF at room temperature for 96 hours, though a reduced sensor response was observed at a higher concentration range, likely due to the adsorption of proteins onto the sensor surface.

Ex vivo studies in harvested mice brain tissue

Encouraged by the capability of multiplexed neural probes for simultaneously monitoring dopamine and serotonin after incubating in rat CSF, we finally evaluated the sensing performance of aptamer functionalized G-FET dopamine and serotonin sensors in *ex vivo* brain tissues harvested from Wild-type C57BL/6J mice. Figures 7A and B show the schematic illustration and optical image of the measurement setup where a multiplexed neural probe is implanted into the mouse's brain tissue and an Ag/AgCl electrode is used as a gate channel. It should be noted that bioresorbable or removable implantation shuttles are typically used for the precise implantation of soft neural probes into targeted brain regions[80]. For those *ex vivo* studies in harvested mice brain tissues, we do not have a concern about brain damage and associated immune responses. Therefore, we fabricated aptamer-gFET sensors on a relatively thick PI substrate (76 μm thick) to avoid the need for implantation shuttles or tungsten stiffeners for precise probe implantation.

To mimic the evoked release and diffusion of dopamine and serotonin in brain tissue by using electrical and/or pharmacological stimulations, the dopamine (10 μM, 2 μL) or serotonin solution (100 nM, 2 μL) was infused into the brain tissue through the injection site by using a Hamilton microsyringe. These concentrations were chosen to represent a physiologically relevant dopamine[81] or serotonin[36] release upon pharmacology and/or electrical stimulations. The electrical response of dopamine and serotonin sensors rapidly changes upon the injection and diffusion of dopamine or serotonin solution into the brain tissue and then slowly decays due to dopamine or serotonin diffusing away from the sensor surface (Figures 7C and D). To further prove the capability of aptamer-functionalized G-FET dopamine and serotonin sensors to record diffusion-related changes in dopamine or serotonin concentration in harvested brain tissue, we performed real-time monitoring of the transfer curves (instead of the source-drain current) upon the injection of dopamine or serotonin solution in harvested mouse's brain tissue (Figures 7E and F). We observed that the transfer curves of dopamine sensors first shifted to the right and then to the left due to the p-doping effect on G-FET upon the conformation change of dopamine aptamer in the presence of target dopamine (Figure 7E). In contrast, the transfer curves of serotonin sensors first shifted to the left and then to the right because the conformal changes of serotonin aptamer resulted in an n-doping effect on G-FET (Figure 7F). With a fixed gate voltage (V_G) of 0 mV, the change of source-drain current (I_{ds}) rapidly increases/decreases and then slowly decays with the injection of dopamine or serotonin solution (Figures 7G and H), which is consistent with the real-time source-drain current monitoring. In our control experiments where the sensor signal changes induced by injecting 2 μL aCSF are much smaller than those caused by the perfusion of 2 μL 100 nM serotonin or 10 μM dopamine in aCSF (Figures S6 and S7). To further mimic the evoked release and diffusion of dopamine or serotonin, the continuous transfer curve monitoring was also performed in brain tissue phantom (0.6 wt% agarose in 1×PBS and soaked in 1×PBS for 24 hours) upon the infusion of dopamine or serotonin solution (Figure S8A). Like the study in harvested brain tissues, the transfer curves of dopamine sensors shift to the right first and then to the left (Figure S8B), while the transfer curves of serotonin sensors shift to the left first and then to the right (Figure S8C). The source-drain current at the fixed gate voltage of 0 mV increases (decreases) first and then shows a slow decay (Figures S8D and E), mainly due to the binding between the aptamer and the target (rapidly increase or decrease) upon the injection of target solution and the diffusion of the target molecules away from the sensor surface (slow decay). Overall, these *ex vivo* studies in harvested mice brain tissue and studies in brain tissue phantom suggest the potential application of aptamer-functionalized multiplexed neural probes for monitoring the evoked release of dopamine and serotonin *in vivo*.

Conclusion

In summary, we developed a soft neural probe for multiplexed monitoring of dopamine and serotonin, two important neurochemicals playing critical roles in mood control, rewarding, motor control, and reinforcement learning. The multiplexed neural probes are developed based on the electrochemically grafted site-selective functionalization of -COOH and -NH_2 onto an ultrasensitive G-FET and the sequential surface functionalization with targeted aptamers. The developed multiplexed neural probes show high sensitivity, molecular

specificity, nearly cellular scale spatial resolution, and minimal crosstalk. The neural probes maintain the ability to perform multiplexed monitoring of dopamine and serotonin after incubating in rat CSF for 96 hours at room temperature. *Ex vivo* studies using harvested mice brain tissue demonstrate the multiplexed monitoring of dopamine and serotonin upon injecting physiologically relevant concentrations of dopamine or serotonin solutions. Future work is needed to develop surface coatings to prevent protein adsorption on the sensor surface and to study the corelease of dopamine and serotonin through *in vivo* studies. Overall, this study opens the door for neuroscientists to study where and how the corelease of multiple neurochemicals modulate the diverse outputs of the brain. The developed multiplexed neural probes can also be adapted to interface with other organs, including spinal cords, hearts, and peripheral nerves, where multiplexed detection is needed.

EXPERIMENTAL SECTION

Materials.

Chemical vapor deposition (CVD)-grown monolayer graphene was purchased from Graphenea. Polymethyl methacrylate (PMMA, inherent viscosity ~1.25 dL/g (lit.), crystalline), acetone (laboratory reagent, ≥99.5%), anisole (Anisole, anhydrous, 99.7%), acetonitrile (ACN, Anhydrous,≥99.8%), hydrochloric acid (HCl, ACS reagent, 37%), tetrabutylammonium hexafluorophosphate ($TBAPF_6$, ACS regent, ≥98%), sodium nitrite ($NaNO_2$ ACS regent, ≥97%), 4-Aminobenzoic acid (p-ABA, ACS regent, ≥99%), p-Phenylenediamine (PPD, 98% (GC)), dimethylaminopropyl)-N-ethylcarbodiimide hydrochloride (EDC), N-Hydroxysulfosuccinimide sodium salt (NHS), bovine serum albumin (BSA), agarose, dopamine (DA), serotonin, norepinephrine (NE), and gamma-aminobutyric acid (GABA) were purchased from Sigma Aldrich. Polydimethylsiloxane (PDMS, Sylgard 184) was purchased from Dow SYLGARD. Rat CSF (RAT01CSF-0104036, gender pooled) was purchased from BioIVT Elevating Science. AZ 5214E, SU8 photoresists were purchased from Integrated Micro Materials. Serotonin aptamer (5′-AmC6-CGA CTG GTA GGC AGA TAG GGG AAG CTG ATT CGA TGC GTG GGT CG-3′) and dopamine aptamer (5′/COOH/CGA CGC CAG TTT GAA GGT TCG TTC GCA GGT GTG GAG TGA CGT CG) were reported by a previous study[58] and purchased from Integrated DNA Technologies, Inc. All of the chemicals and materials were used without further purification after purchase.

1. Fabrication and electrochemical cleaning of G-FETs

1.1 Preparation of graphene patterns

A piece of CVD-grown monolayer graphene (Graphenea) was first coated with PMMA A4 solution (4 g PMMA dissolved in 96 g anisole) to get the PMMA/graphene/Cu stack, which was then heated at 180 °C for 5 min and slowly cooled down to room temperature. The PMMA/graphene/Cu was further cut into small pieces and floated on the surface of the copper etchant for 5 mins to remove the Cu film. After that, the obtained PMMA/graphene film was transferred into the 0.1 M HCl for 10 mins and then washed with deionized (DI) water three times. A piece of Si wafer was then used to pick up the transferred PMMA/graphene film. After drying in the air overnight at room temperature, PMMA A2 solution (2

g PMMA in 98 g anisole) was applied onto the surface of the PMMA/graphene/Si to release the possible wrinkles in graphene. Then, PMMA/graphene/Si was immersed into acetone for 4 h to remove the PMMA. The obtained graphene/Si was spin-coated (at 500 rpm for 10 s followed with 1500 rpm for 25 s, acceleration of 300 rmp/s) with the photoresist (AZ5214), followed by baking at 95 °C for 3 min on a hotplate. A predesigned mask was used to form desired patterns on the graphene surface by oxygen plasma. Finally, the graphene pattern with a size of 60 μm × 60 μm was obtained by removing the photoresist with acetone.

1.2 Preparation of source-drain electrodes

A mixture of PDMS elastomer and curing reagent (10:1 ratio) was first spin-coated on a glass slide (75 mm × 50 mm), which was then cured in a 70 °C oven for 10 min. After that, the PI film was laminated onto the semi-cured PDMS surface, followed by another 50 min curing at 70 °C. Then, the PI film was spin-coated with AZ5214 photoresist and baked at 95 °C for 3 min on a hotplate. With exposure to UV light through a designed mask and the development, interdigitated patterns were formed on the surface of PI film. An RF sputter (AJA Orion-8) was used to deposit Cr with 15 nm thickness and Au with 90 nm thickness on top of the patterned PI film. A lift-off process was carried out to form the source-drain electrodes on the soft PI film.

1.3 Graphene transfer to source-drain electrodes and device encapsulation

The obtained graphene patterns were first coated with PMMA A4 solution to form a PMMA/graphene/Si stack, which was then heated at 180 °C for 5 min and cooled down to room temperature naturally. Next, the above stack was immersed in 1 mM NaOH solution until the PMMA/graphene pattern stack detached from the Si wafer surface and floated on the solution. The PMMA/graphene pattern was washed with DI water 3 times and then transferred on the PI film containing source and drain contact pads under a microscope. Similarly, after overnight drying in the air, the PMMA A2 solution was dropped on the PI film to release the possible wrinkles in graphene. After immersing the PI film covered by PMMA/graphene pattern stack into acetone for 4 h, the PMMA layer can be removed to get the graphene pattern on the pre-constructed source and drain contact pads. Finally, the source and drain electrodes were encapsulated with SU8 (2000.5, MicroChem) following the standard photolithography protocol. The final thickness of the SU8 layer and the active sensing area of graphene is 0.8 μm and 50 μm × 50 μm, respectively.

1.4 Electrochemical cleaning of the G-FETs

The fabricated G-FETs were first cleaned by using an electrochemical method[65]. More specifically, a non-aqueous electrolyte containing acetonitrile (Sigma Aldrich) and 100 mM tetrabutylammonium hexafluorophosphate ($TBAPF_6$, Sigma Aldrich) was used to perform the electrochemical cleaning using an Autolab potentiostat (Autolab PGSTAT128N). The G-FET was used as the working electrode (WE) with a platinum wire as a counter electrode (CE) and Ag/AgCl electrode as a reference electrode (RE). The CV was performed under the potential window from −0.7 to 0 V vs. Ag/AgCl at a scan rate of 0.5 V s^{-1} for 100 cycles. After the electrochemical treatment, the cleaned G-FET was rinsed several times using pure acetonitrile and DI water to remove the residual electrolyte from the graphene surface.

2. Surface functionalization of G-FETs

2.1 Electrochemical grafting -COOH group on the graphene surface

The classic diazonium reaction was used for electrochemical grafting of the -COOH group on the graphene surface of G-FET. First, a 10 mL 2 mM $NaNO_2$ solution drops into 10 mL 2 mM p-aminobenzoic acid (p-ABA) solution in 1 M HCl solution in 30 mins. The mixed solution was then degassed under nitrogen flow for 5 mins and left to react in an ice water bath for another 10 mins for the formation of the diazonium salt (ClN_{2+}-Ph-COOH). After that, the G-FET was immersed into the above mixture solution to serve as the working electrode. Saturated Ag/AgCl electrode and Pt electrode were used as the reference electrode and counter electrode, respectively. A CV scan was used to graft -Ph-COOH onto the graphene surface at a scan rate of 100 mV s^{-1} within a voltage window of −0.6 V to 0.5 V. Different scan cycles were performed to optimize the electrochemical grafting process to achieve the fully covered graphene surface with -COOH group. Finally, the -COOH functionalized G-FET was thoroughly rinsed with acetonitrile and DI water to remove the nonspecifically adsorbed substances.

2.2 Electrochemical grafting -NH_2 group on the graphene surface

The diazonium reaction was also used for electrochemical grafting of the -NH_2 group on the graphene surface of G-FET following a similar protocol as that of -COOH electrografting . Here, 10 mL, 4 mM $NaNO_2$ solution was first dropwise into 10 mM phenylenediamine (PPD) in 1 M HCl solution. After degassing using nitrogen flow for 5 mins, and then the mixed solution was left in an ice water bath for 10 min to form diazonium salt (ClN_{2+}-Ph-NH_2). CV scans were performed at a scan of 100 mV s^{-1} in the potential window of −0.6 V to 0.5 V for 5 cycles to graft -NH_2 group on the graphene surfaces of G-FET. Finally, the obtained -NH_2-grafted G-FET was thoroughly rinsed with acetonitrile and ultrapure DI water to remove the nonspecifically adsorbed substances.

2.3 Surface functionalization of aptamers through EDC-NHS reactions

For the functionalization of G-FETs with serotonin aptamers, the electrografted G-FETs with -COOH groups were incubated in the PBS solution containing 6 mM EDC, 3 mM NHS, and 3 μM amino group modified serotonin aptamer (5′-AmC6-CGA CTG GTA GGC AGA TAG GGG AAG CTG ATT CGA TGC GTG GGT CG-3′) at room temperature for 4 h. After that, the functionalized G-FETs linked with serotonin aptamers were washed with DI water and dried with N_2 gas.

For the functionalization of G-FETs with dopamine aptamers, the electrografted G-FETs with -NH_2 groups were first incubated in the 1× PBS solution containing 6 mM EDC, 3 mM NHS, and 3 μM carboxyl group modified dopamine aptamer (5′/COOH/CGA CGC CAG TTT GAA GGT TCG TTC GCA GGT GTG GAG TGA CGT CG,) at room temperature for 4 h. After that, the functionalized G-FETs linked with dopamine aptamers were washed with DI water and dried with N_2 gas.

3. Materials characterization and sensing performance evaluation

3.1 Materials characterization

The pattern and graphene microstructure of the prepared G-FETs were characterized by scanning electron microscopy (SEM; Teneo LV SEM equipped with energy-dispersive X-ray spectroscopy (EDS) detector), atomic force microscopy (AFM; mfp-3D operating in conventional intermittent contact, Asylum Research), and Raman spectroscopy (Renishaw InVia Raman microscope at 575 nm with 10% laser power). Electrical measurement was performed with the Keysight B1500A Semiconductor Analyzer and probe station.

3.2 Sensing performance evaluation

3.2.1 Real-time response of the functionalized G-FETs—The real-time response of the functionalized G-FETs with serotonin aptamers was performed using the Keithley B1500A Semiconductor Analyzer and probe station. Each time, 20 μL test solution was put on the sensing area of G-FET to record the response. After that, the test solution was quickly removed using Kimwipes, and the next test solution was added immediately using a second pipette. A series of freshly prepared serotonin solutions were used to evaluate the sensing performance of the fabricated G-FETs with serotonin aptamer. Similarly, the real-time response of G-FETs with dopamine aptamer was evaluated by gradually adding freshly prepared dopamine solution.

3.2.2 Selectivity of the functionalized G-FETs sensor—The selectivity of the functionalized G-FETs with dopamine or serotonin aptamers was evaluated by recording the electrical response when the G-FETs were exposed to different neurotransmitters, such as dopamine, serotonin, norepinephrine, and gamma-aminobutyric acid.

4. Tissue collection

Adult C57BL/6J mice obtained from Jackson laboratories were used for all experiments. Brain tissue was harvested after transcardial perfusion with aCSF (LRE-S-LSG-1000-1, EcoCyte Bioscience). Mice were first anesthetized with 5% isoflurane in an induction chamber and then held under anesthesia with a nose cone throughout the procedure. An incision was made along the ventral surface of the mouse to expose the diaphragm, which was then separated from the rib cage. The rib cage was excised to expose the heart. Using a pair of blunt forceps, the heart was stabilized, and a needle for perfusion was inserted into the left ventricle. A small incision was then made in the right atrium of the heart, and 15 mL of aCSF was perfused through the animal. Once perfused, the mice were decapitated, and the dorsal surface of the skull was exposed with a midline incision through the skin. The skull is then opened to expose the brain, which is subsequently extracted and placed in aCSF. All experiments performed were approved by the University of Connecticut Institutional Animal Care and Use Committee Institutional Animal Care and Use Committee (IACUC).

5. Statistics

Experimental data are expressed as the mean ± standard deviation (SD). For two-group comparisons, statistical significance was determined by one-tailed Student's t tests. $P < 0.05$ was considered statistically significant. The software used for statistical analysis was OriginLab.

Supplementary Material

Refer to Web version on PubMed Central for supplementary material.

Acknowledgement

We thank Gavin Fennell for proofreading the manuscript. This work is supported by NIH BRAIN Initiative RF1NS118287 (to Y.Z.).

Reference:

1. Myhrer T, Neurotransmitter systems involved in learning and memory in the rat: a meta-analysis based on studies of four behavioral tasks. Brain Res Brain Res Rev 2003, 41 (2–3), 268–87. [PubMed: 12663083]
2. Wise RA, Dopamine, learning and motivation. Nat Rev Neurosci 2004, 5 (6), 483–94. [PubMed: 15152198]
3. Webster R, Neurotransmitters, drugs and brain function. John Wiley & Sons: 2001.
4. Ngernsutivorakul T; White TS; Kennedy RT, Microfabricated Probes for Studying Brain Chemistry: A Review. Chemphyschem 2018, 19 (10), 1128–1142. [PubMed: 29405568]
5. Jankovic J, Parkinson's disease tremors and serotonin. Brain 2018, 141 (3), 624–626. [PubMed: 30063797]
6. Joling M; van den Heuvel OA; Berendse HW; Booij J; Vriend C, Serotonin transporter binding and anxiety symptoms in Parkinson's disease. J Neurol Neurosurg Psychiatry 2018, 89 (1), 89–94. [PubMed: 28899958]
7. Sitte HH; Pifl C; Rajput AH; Hortnagl H; Tong J; Lloyd GK; Kish SJ; Hornykiewicz O, Dopamine and noradrenaline, but not serotonin, in the human claustrum are greatly reduced in patients with Parkinson's disease: possible functional implications. Eur J Neurosci 2017, 45 (10), 1356. [PubMed: 28523903]
8. Pagano G; Niccolini F; Fusar-Poli P; Politis M, Serotonin transporter in Parkinson's disease: A meta-analysis of positron emission tomography studies. Ann Neurol 2017, 81 (2), 171–180. [PubMed: 28019672]
9. Stahl SM, Parkinson's disease psychosis as a serotonin-dopamine imbalance syndrome. CNS Spectr 2016, 21 (5), 355–359. [PubMed: 27686027]
10. Blum R; Lesch KP, Parkinson's disease, anxious depression and serotonin--zooming in on hippocampal neurogenesis. J Neurochem 2015, 135 (3), 441–4. [PubMed: 26382574]
11. McCutcheon RA; Abi-Dargham A; Howes OD, Schizophrenia, Dopamine and the Striatum: From Biology to Symptoms. Trends Neurosci 2019, 42 (3), 205–220. [PubMed: 30621912]
12. Francis PT, Glutamatergic systems in Alzheimer's disease. Int J Geriatr Psychiatry 2003, 18 (Suppl 1), S15–21. [PubMed: 12973746]
13. Saunders A; Granger AJ; Sabatini BL, Corelease of acetylcholine and GABA from cholinergic forebrain neurons. Elife 2015, 4, e06412.
14. Root DH; Mejias-Aponte CA; Zhang S; Wang HL; Hoffman AF; Lupica CR; Morales M, Single rodent mesohabenular axons release glutamate and GABA. Nat Neurosci 2014, 17 (11), 1543–51. [PubMed: 25242304]

15. Shabel SJ; Proulx CD; Piriz J; Malinow R, Mood regulation. GABA/glutamate co-release controls habenula output and is modified by antidepressant treatment. Science 2014, 345 (6203), 1494–8. [PubMed: 25237099]

16. Barker DJ; Root DH; Zhang S; Morales M, Multiplexed neurochemical signaling by neurons of the ventral tegmental area. J Chem Neuroanat 2016, 73, 33–42. [PubMed: 26763116]

17. Yoo JH; Zell V; Gutierrez-Reed N; Wu J; Ressler R; Shenasa MA; Johnson AB; Fife KH; Faget L; Hnasko TS Nat Commun. 2016, 7, 13697. [PubMed: 27976722]

18. Zhou FM; Liang Y; Salas R; Zhang L; De Biasi M; Dani JA, Corelease of dopamine and serotonin from striatal dopamine terminals. Neuron 2005, 46 (1), 65–74. [PubMed: 15820694]

19. Eskenazi D; Malave L; Mingote S; Yetnikoff L; Ztaou S; Velicu V; Rayport S; Chuhma N Front. Neural Circuits. 2021, 15, 665386. [PubMed: 34093138]

20. Patriarchi T; Cho JR; Merten K; Howe MW; Marley A; Xiong WH; Folk RW; Broussard GJ; Liang R; Jang MJ; Zhong H; Dombeck D; von Zastrow M; Nimmerjahn A; Gradinaru V; Williams JT; Tian L, Ultrafast neuronal imaging of dopamine dynamics with designed genetically encoded sensors. Science 2018, 360 (6396), eaat4422. [PubMed: 29853555]

21. Xu C; Wu F; Yu P; Mao L, In Vivo Electrochemical Sensors for Neurochemicals: Recent Update. ACS Sens 2019, 4 (12), 3102–3118. [PubMed: 31718157]

22. Tan C; Robbins EM; Wu B; Cui XT, Recent Advances in In Vivo Neurochemical Monitoring. Micromachines (Basel) 2021, 12 (2).

23. Drevets WC; Price JC; Kupfer DJ; Kinahan PE; Lopresti B; Holt D; Mathis C, PET measures of amphetamine-induced dopamine release in ventral versus dorsal striatum. Neuropsychopharmacology 1999, 21 (6), 694–709. [PubMed: 10633475]

24. Moody AS; Sharma B, Multi-metal, Multi-wavelength Surface-Enhanced Raman Spectroscopy Detection of Neurotransmitters. ACS Chem Neurosci 2018, 9 (6), 1380–1387. [PubMed: 29601719]

25. Bell SE; Park I; Rubakhin SS; Bashir R; Vlasov Y; Sweedler JV, Droplet Microfluidics with MALDI-MS Detection: The Effects of Oil Phases in GABA Analysis. ACS Measurement Science Au 2021, 1(3), 147–156. [PubMed: 34939077]

26. Leopold AV; Shcherbakova DM; Verkhusha VV, Fluorescent Biosensors for Neurotransmission and Neuromodulation: Engineering and Applications. Front Cell Neurosci 2019, 13, 474. [PubMed: 31708747]

27. Liang R; Broussard GJ; Tian L, Imaging chemical neurotransmission with genetically encoded fluorescent sensors. ACS Chem Neurosci 2015, 6 (1), 84–93. [PubMed: 25565280]

28. Nalewajko E; Bort Ramirez R; Kojlo A, Determination of dopamine by flow-injection analysis coupled with luminol-hexacyanoferrate(III) chemiluminescence detection. J Pharm Biomed Anal 2004, 36 (1), 219–23. [PubMed: 15351069]

29. Zibaii M; Latifi H; Asadollahi A; Bayat AH; Dargahi L; Haghparast A, Label free fiber optic apta-biosensor for in-vitro detection of dopamine. Journal of Lightwave Technology 2016, 34 (19), 4516–4524.

30. Lin Y; Chen C; Wang C; Pu F; Ren J; Qu X, Silver nanoprobe for sensitive and selective colorimetric detection of dopamine via robust Ag-catechol interaction. Chem Commun (Camb) 2011, 47 (4), 1181–3. [PubMed: 21082144]

31. Xiao T; Wu F; Hao J; Zhang M; Yu P; Mao L, In Vivo Analysis with Electrochemical Sensors and Biosensors. Anal Chem 2017, 89 (1), 300–313. [PubMed: 28105815]

32. Xue Y; Ji W; Jiang Y; Yu P; Mao L, Deep Learning for Voltammetric Sensing in a Living Animal Brain. Angew Chem Int Ed Engl 2021, 60 (44), 23777–23783. [PubMed: 34410032]

33. Abdalla A; Atcherley CW; Pathirathna P; Samaranayake S; Qiang B; Pena E; Morgan SL; Heien ML; Hashemi P, In Vivo Ambient Serotonin Measurements at Carbon-Fiber Microelectrodes. Anal Chem 2017, 89 (18), 9703–9711. [PubMed: 28795565]

34. Venton BJ; Cao Q, Fundamentals of fast-scan cyclic voltammetry for dopamine detection. Analyst 2020, 145 (4), 1158–1168. [PubMed: 31922176]

35. Castagnola E; Garg R; Rastogi SK; Cohen-Karni T; Cui XT, 3D fuzzy graphene microelectrode array for dopamine sensing at sub-cellular spatial resolution. Biosens Bioelectron 2021, 191, 113440. [PubMed: 34171734]

36. Shin H; Oh Y; Park C; Kang Y; Cho HU; Blaha CD; Bennet KE; Heien ML; Kim IY; Lee KH; Jang DP, Sensitive and Selective Measurement of Serotonin in Vivo Using Fast Cyclic Square-Wave Voltammetry. Anal Chem 2020, 92 (1), 774–781. [PubMed: 31789495]
37. Westerink RH, Exocytosis: using amperometry to study presynaptic mechanisms of neurotoxicity. Neurotoxicology 2004, 25 (3), 461–70. [PubMed: 15019309]
38. Zhao XE; Suo YR, Simultaneous determination of monoamine and amino acid neurotransmitters in rat endbrain tissues by pre-column derivatization with high-performance liquid chromatographic fluorescence detection and mass spectrometric identification. Talanta 2008, 76 (3), 690–7. [PubMed: 18585341]
39. Neumann EK; Comi TJ; Spegazzini N; Mitchell JW; Rubakhin SS; Gillette MU; Bhargava R; Sweedler JV, Multimodal Chemical Analysis of the Brain by High Mass Resolution Mass Spectrometry and Infrared Spectroscopic Imaging. Anal Chem 2018, 90 (19), 11572–11580. [PubMed: 30188687]
40. Zestos AG; Kennedy RT, Microdialysis Coupled with LC-MS/MS for In Vivo Neurochemical Monitoring. AAPS J 2017, 19 (5), 1284–1293. [PubMed: 28660399]
41. Lee WH; Slaney TR; Hower RW; Kennedy RT, Microfabricated sampling probes for in vivo monitoring of neurotransmitters. Anal Chem 2013, 85 (8), 3828–31. [PubMed: 23547793]
42. Zhou Y; Wong JM; Mabrouk OS; Kennedy RT, Reducing adsorption to improve recovery and in vivo detection of neuropeptides by microdialysis with LC-MS. Anal Chem 2015, 87 (19), 9802–9. [PubMed: 26351736]
43. Al-Hasani R; Wong JT; Mabrouk OS; McCall JG; Schmitz GP; Porter-Stransky KA; Aragona BJ; Kennedy RT; Bruchas MR, In vivo detection of optically-evoked opioid peptide release. Elife 2018, 7, e36520. [PubMed: 30175957]
44. Wu G; Heck I; Zhang N; Phaup G; Zhang X; Wu Y; Stalla DE; Weng Z; Sun H; Li H; Zhang Z; Ding S; Li DP; Zhang Y, Wireless, battery-free push-pull microsystem for membrane-free neurochemical sampling in freely moving animals. Sci Adv 2022, 8 (8), eabn2277. [PubMed: 35196090]
45. Pradhan T; Jung HS; Jang JH; Kim TW; Kang C; Kim JS, Chemical sensing of neurotransmitters. Chem Soc Rev 2014, 43 (13), 4684–713. [PubMed: 24736802]
46. Zhang Y; Jiang N; Yetisen AK, Brain neurochemical monitoring. Biosens Bioelectron 2021, 189, 113351. [PubMed: 34049083]
47. Wu Z; Lin D; Li Y, Pushing the frontiers: tools for monitoring neurotransmitters and neuromodulators. Nat Rev Neurosci 2022, 23 (5), 257–274. [PubMed: 35361961]
48. Moran RJ; Kishida KT; Lohrenz T; Saez I; Laxton AW; Witcher MR; Tatter SB; Ellis TL; Phillips PE; Dayan P; Montague PR, The Protective Action Encoding of Serotonin Transients in the Human Brain. Neuropsychopharmacology 2018, 43 (6), 1425–1435. [PubMed: 29297512]
49. Movassaghi CS; Perrotta KA; Yang H; Iyer R; Cheng X; Dagher M; Fillol MA; Andrews AM, Simultaneous serotonin and dopamine monitoring across timescales by rapid pulse voltammetry with partial least squares regression. Anal Bioanal Chem 2021, 413 (27), 6747–6767. [PubMed: 34686897]
50. Clark JJ; Sandberg SG; Wanat MJ; Gan JO; Horne EA; Hart AS; Akers CA; Parker JG; Willuhn I; Martinez V; Evans SB; Stella N; Phillips PE, Chronic microsensors for longitudinal, subsecond dopamine detection in behaving animals. Nat Methods 2010, 7 (2), 126–9. [PubMed: 20037591]
51. Schwerdt HN; Zhang E; Kim MJ; Yoshida T; Stanwicks L; Amemori S; Dagdeviren HE; Langer R; Cima MJ; Graybiel AM, Cellular-scale probes enable stable chronic subsecond monitoring of dopamine neurochemicals in a rodent model. Commun Biol 2018, 1, 144. [PubMed: 30272020]
52. Puthongkham P; Venton BJ, Recent advances in fast-scan cyclic voltammetry. Analyst 2020, 145 (4), 1087–1102. [PubMed: 31922162]
53. Chefer VI; Thompson AC; Zapata A; Shippenberg TS, Overview of brain microdialysis. Curr Protoc Neurosci 2009, Chapter 7, Unit7 1.
54. Anderzhanova E; Wotjak CT, Brain microdialysis and its applications in experimental neurochemistry. Cell Tissue Res 2013, 354 (1), 27–39. [PubMed: 24022232]
55. Sun F; Zeng J; Jing M; Zhou J; Feng J; Owen SF; Luo Y; Li F; Wang H; Yamaguchi T; Yong Z; Gao Y; Peng W; Wang L; Zhang S; Du J; Lin D; Xu M; Kreitzer AC; Cui G; Li Y, A Genetically

Encoded Fluorescent Sensor Enables Rapid and Specific Detection of Dopamine in Flies, Fish, and Mice. Cell 2018, 174 (2), 481–496 e19. [PubMed: 30007419]

56. Feng J; Zhang C; Lischinsky JE; Jing M; Zhou J; Wang H; Zhang Y; Dong A; Wu Z; Wu H; Chen W; Zhang P; Zou J; Hires SA; Zhu JJ; Cui G; Lin D; Du J; Li Y, A Genetically Encoded Fluorescent Sensor for Rapid and Specific In Vivo Detection of Norepinephrine. Neuron 2019, 102 (4), 745–761 e8. [PubMed: 30922875]
57. Sabatini BL; Tian L, Imaging Neurotransmitter and Neuromodulator Dynamics In Vivo with Genetically Encoded Indicators. Neuron 2020, 108 (1), 17–32. [PubMed: 33058762]
58. Nakatsuka N; Yang KA; Abendroth JM; Cheung KM; Xu X; Yang H; Zhao C; Zhu B; Rim YS; Yang Y; Weiss PS; Stojanovic MN; Andrews AM, Aptamerfield-effect transistors overcome Debye length limitations for small-molecule sensing. Science 2018, 362 (6412), 319–324. [PubMed: 30190311]
59. Zhao C; Cheung KM; Huang IW; Yang H; Nakatsuka N; Liu W; Cao Y; Man T; Weiss PS; Monbouquette HG; Andrews AM, Implantable aptamer-field-effect transistor neuroprobes for in vivo neurotransmitter monitoring. Sci Adv 2021, 7 (48), eabj7422. [PubMed: 34818033]
60. Wu G; Zhang N; Matarasso A; Heck I; Li H; Lu W; Phaup JG; Schneider MJ; Wu Y; Weng Z; Sun H; Gao Z; Zhang X; Sandberg SG; Parvin D; Seaholm E; Islam SK; Wang X; Phillips PEM; Castro DC; Ding S; Li DP; Bruchas MR; Zhang Y, Implantable Aptamer-Graphene Microtransistors for Real-Time Monitoring of Neurochemical Release in Vivo. Nano Lett 2022, 22 (9), 3668–3677. [PubMed: 35439419]
61. Lu L; Gutruf P; Xia L; Bhatti DL; Wang X; Vazquez-Guardado A; Ning X; Shen X; Sang T; Ma R; Pakeltis G; Sobczak G; Zhang H; Seo DO; Xue M; Yin L; Chanda D; Sheng X; Bruchas MR; Rogers JA, Wireless optoelectronic photometers for monitoring neuronal dynamics in the deep brain. Proc Natl Acad Sci U S A 2018, 115 (7), E1374–E1383. [PubMed: 29378934]
62. Du M; Huang L; Zheng J; Xi Y; Dai Y; Zhang W; Yan W; Tao G; Qiu J; So KF; Ren C; Zhou S, Flexible Fiber Probe for Efficient Neural Stimulation and Detection. Adv Sci (Weinh) 2020, 7 (15), 2001410. [PubMed: 32775173]
63. Cho Y; Park S; Lee J; Yu KJ, Emerging Materials and Technologies with Applications in Flexible Neural Implants: A Comprehensive Review of Current Issues with Neural Devices. Adv Mater 2021, 33 (47), e2005786. [PubMed: 34050691]
64. Luan L; Wei X; Zhao Z; Siegel JJ; Potnis O; Tuppen CA; Lin S; Kazmi S; Fowler RA; Holloway S; Dunn AK; Chitwood RA; Xie C, Ultraflexible nanoelectronic probes form reliable, glial scar-free neural integration. Sci Adv 2017, 3 (2), e1601966. [PubMed: 28246640]
65. Park B; Huh JN; Lee WS; Bae I-G, Simple and rapid cleaning of graphenes with a 'bubble-free'electrochemical treatment. Journal of Materials Chemistry C 2018, 6 (9), 2234–2244.
66. Fu W; Jiang L; van Geest EP; Lima LM; Schneider GF, Sensing at the Surface of Graphene Field-Effect Transistors. Adv Mater 2017, 29 (6), 1603610.
67. Hwang MT; Heiranian M; Kim Y; You S; Leem J; Taqieddin A; Faramarzi V; Jing Y; Park I; van der Zande AM; Nam S; Aluru NR; Bashir R, Ultrasensitive detection of nucleic acids using deformed graphene channel field effect biosensors. Nat Commun 2020, 11 (1), 1543. [PubMed: 32210235]
68. Beraud A; Sauvage M; Bazan CM; Tie M; Bencherif A; Bouilly D, Graphene field-effect transistors as bioanalytical sensors: design, operation and performance. Analyst 2021, 146 (2), 403–428. [PubMed: 33215184]
69. Wang C; Yan Q; Liu HB; Zhou XH; Xiao SJ, Different EDC/NHS activation mechanisms between PAA and PMAA brushes and the following amidation reactions. Langmuir 2011, 27 (19), 12058–68. [PubMed: 21853994]
70. Wickramathilaka MP; Tao BY, Characterization of covalent crosslinking strategies for synthesizing DNA-based bioconjugates. J Biol Eng 2019, 13, 63. [PubMed: 31333759]
71. Kesler V; Murmann B; Soh HT, Going beyond the Debye Length: Overcoming Charge Screening Limitations in Next-Generation Bioelectronic Sensors. ACS Nano 2020, 14 (12), 16194–16201. [PubMed: 33226776]
72. Gotrik MR; Feagin TA; Csordas AT; Nakamoto MA; Soh HT, Advancements in Aptamer Discovery Technologies. Acc Chem Res 2016, 49 (9), 1903–10. [PubMed: 27526193]

73. Rangel AE; Hariri AA; Eisenstein M; Soh HT, Engineering Aptamer Switches for Multifunctional Stimulus-Responsive Nanosystems. Adv Mater 2020, 32 (50), e2003704. [PubMed: 33165999]
74. Belanger D; Pinson J, Electrografting: a powerful method for surface modification. Chem Soc Rev 2011, 40 (7), 3995–4048. [PubMed: 21503288]
75. Eckmann A; Felten A; Mishchenko A; Britnell L; Krupke R; Novoselov KS; Casiraghi C, Probing the nature of defects in graphene by Raman spectroscopy. Nano Lett 2012, 12 (8), 3925–30. [PubMed: 22764888]
76. Malard L; Pimenta MA; Dresselhaus G; Dresselhaus M, Raman spectroscopy in graphene. Physics reports 2009, 473 (5–6), 51–87.
77. Artigas F; Sarrias MJ; Martinez E; Gelpi E, Serotonin in body fluids: characterization of human plasmatic and cerebrospinal fluid pools by means of a new HPLC method. Life Sci 1985, 37 (5), 441–7. [PubMed: 3160903]
78. Roberts JG; Sombers LA, Fast-Scan Cyclic Voltammetry: Chemical Sensing in the Brain and Beyond. Anal Chem 2018, 90 (1), 490–504. [PubMed: 29182309]
79. Zhao F; Liu Y; Dong H; Feng S; Shi G; Lin L; Tian Y, An Electrochemophysiological Microarray for Real-Time Monitoring and Quantification of Multiple Ions in the Brain of a Freely Moving Rat. Angew Chem Int Ed Engl 2020, 59 (26), 10426–10430. [PubMed: 32190959]
80. Apollo NV; Murphy B; Prezelski K; Driscoll N; Richardson AG; Lucas TH; Vitale F, Gels, jets, mosquitoes, and magnets: a review of implantation strategies for soft neural probes. J Neural Eng 2020, 17 (4), 041002. [PubMed: 32759476]
81. Ngo KT; Varner EL; Michael AC; Weber SG, Monitoring Dopamine Responses to Potassium Ion and Nomifensine by in Vivo Microdialysis with Online Liquid Chromatography at One-Minute Resolution. ACS Chem Neurosci 2017, 8 (2), 329–338. [PubMed: 28094974]

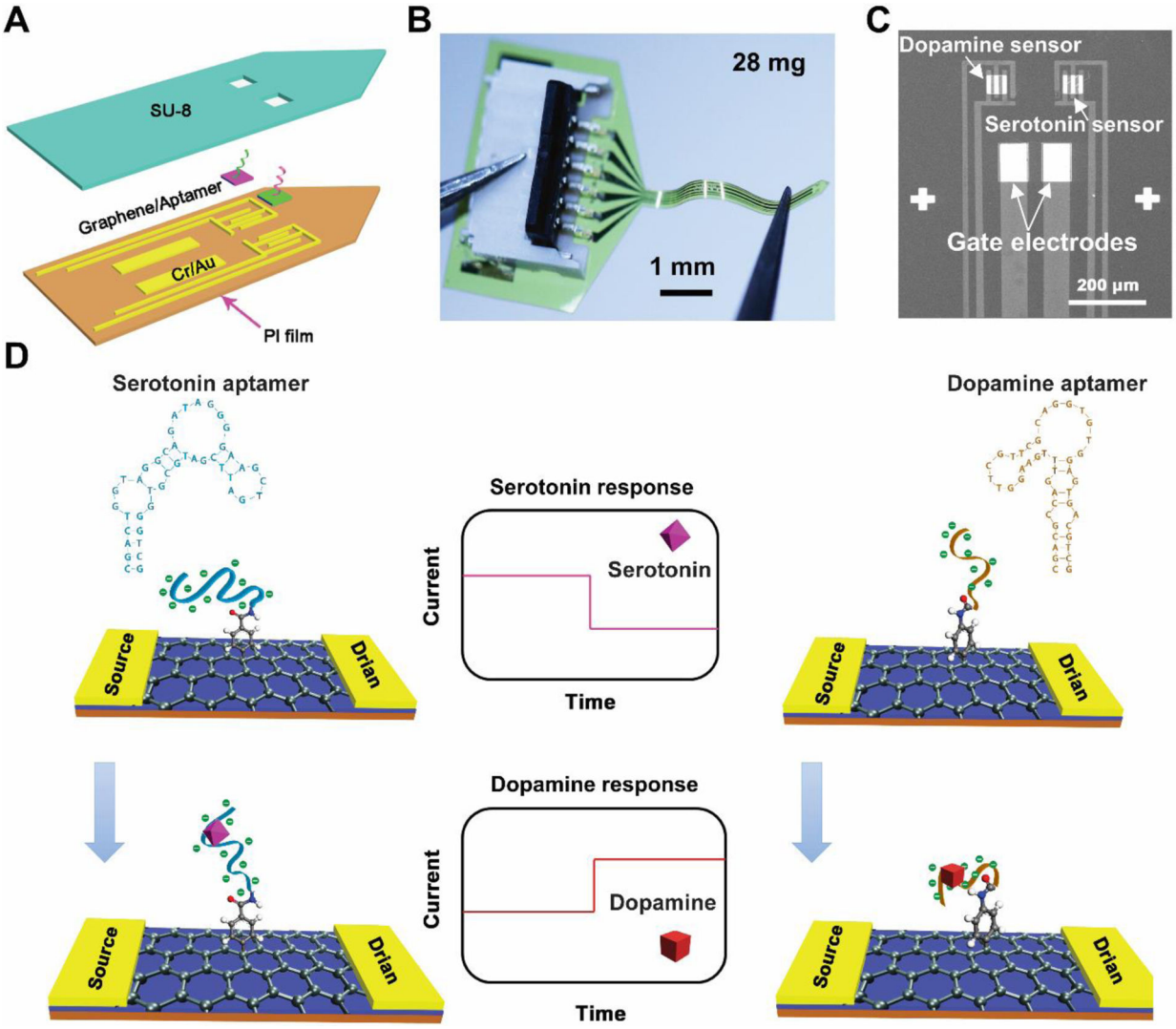

Fig. 1. Design, fabrication, and working principle of G-FETs for multiplexed neurochemical monitoring.

(**A**) Schematic illustration and (**B**) Optical images of the G-FETs probe fabricated on (left) 7.6 μm PI (28 mg) for multiplexed neurochemical sensing. (**C**) SEM image of a representative soft neural probe that consists of two G-FETs, with each G-FET at a nearly cellular-scale dimension (50 μm × 50 μm). (**D**) Working principles of G-FETs for multiplexed neurochemical monitoring. The graphene surfaces of the two side-by-side G-FETs are selectively functionalized with -COOH and -NH_2 groups through electrochemical-grafting methods. The electrografted -COOH and -NH_2 groups serve as linkers to functionalize two aptamers with different functional groups (-NH_2 and -COOH) through the EDC/NHS reactions. When dopamine and serotonin bind with the target-specific aptamer, it will cause the conformational change of the functionalized aptamers on the graphene, changing the doping state of the graphene, and leading to a measurable source-drain current change of the G-FETs.

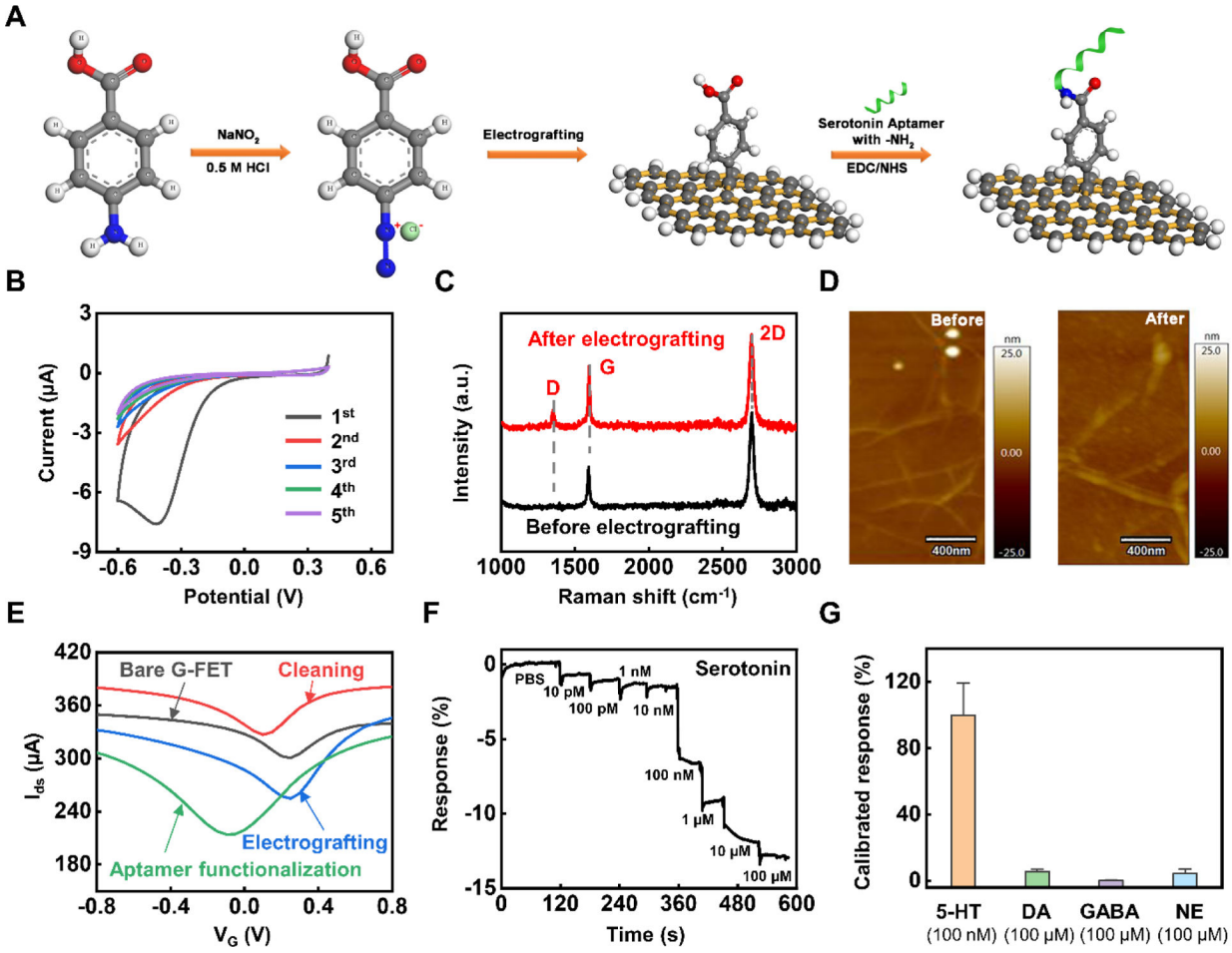

Fig. 2. Electrografting of -COOH group and functionalization of G-FET with serotonin aptamer.

(**A**) Schematic illustration of the electrografting of -COOH group on graphene surface through diazonium reaction and the functionalization of serotonin aptamer through EDC/NHS reactions. (**B**) CV curves of the electrografting process to introduce -COOH group on the graphene surface. (**C**) Raman spectrum of graphene surface before and after electrografting. (**D**) AFM images of graphene surface before and after electro grafting with -COOH group. (**E**) Transfer curves of fabricated G-FETs after different processing steps, including cleaning, electrografting, and aptamer functionalization. V_{ds} = 200 mV. (**F**) The real-time source-drain current response of the G-FET serotonin sensor upon exposure to 1× PBS solution containing serotonin with different concentrations: 10 pM, 100 pM, 1 nM, 10 nM, 100 nM, 1 μM, 10 μM, and 100 μM. The current response is defined as $\Delta I_{ds}/I_0 \times 100\%$, where ΔI_{ds} and I_0 are the change of the source-drain current in the presence of the target and the initial signal without the target, respectively. V_{ds} = 100 mV; V_G = 0 mV. (**G**) Selectivity of serotonin sensor. 5-HT: Serotonin; DA: Dopamine; NE: Norepinephrine; GABA: Gamma-aminobutyric acid.

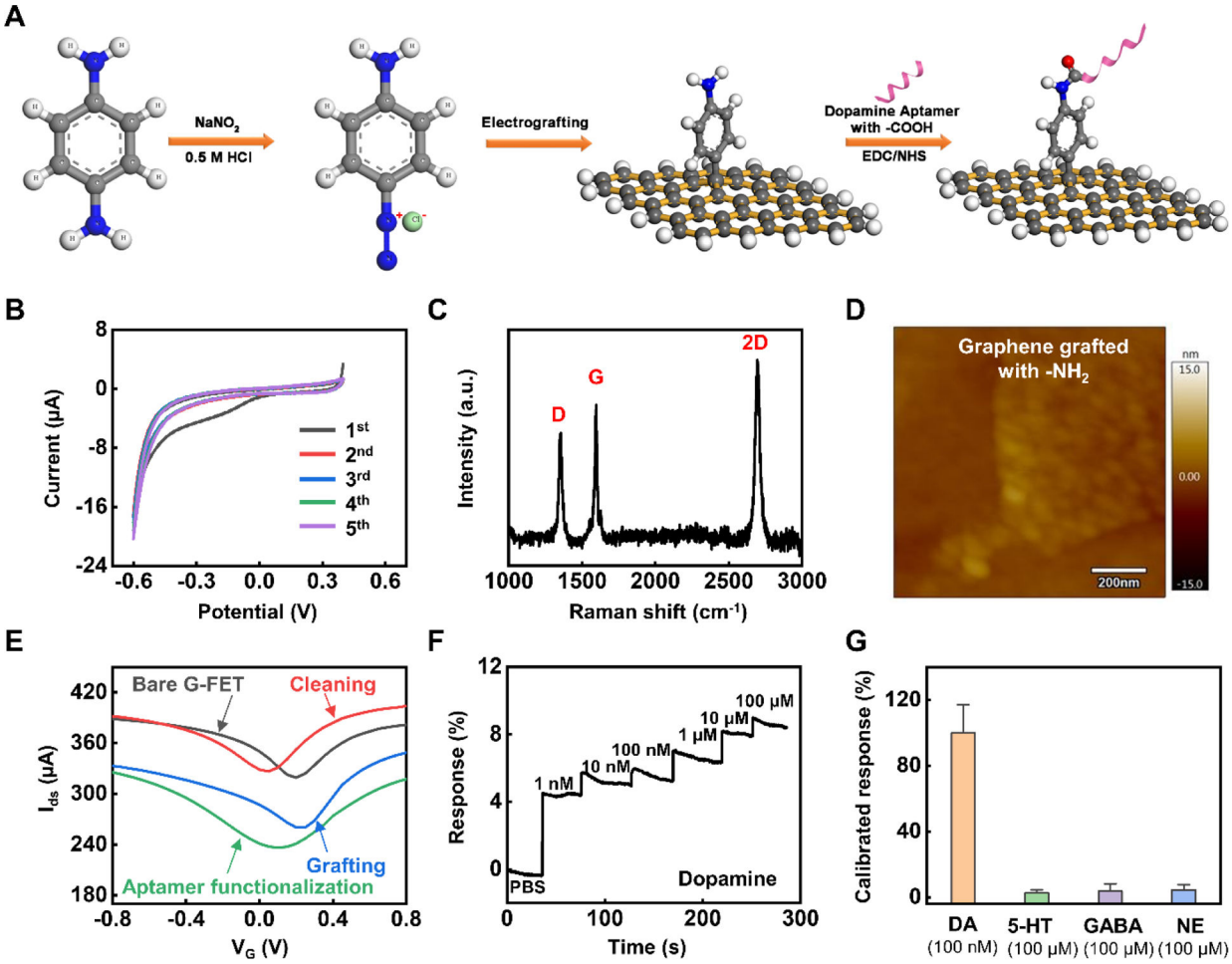

Fig. 3. Electrografting of -NH_2 group and functionalization of G-FET with dopamine aptamer.

(**A**) Schematic illustration of the electrografting of -NH_2 group on graphene surface through diazonium reaction and the functionalization of dopamine aptamer through EDC/NHS reactions. (**B**) CV curves of the electrografting process to introduce -NH_2 group on graphene. (**C**) Raman spectrum of the graphene surface after electrografting with -NH_2 group. (**D**) AFM image of graphene surface electrografted with -NH_2 group. (**E**) Transfer curves of bare G-FET, cleaned G-FET, and G-FET after electrografting (-NH_2 group) and dopamine aptamer functionalization. V_{ds} = 200 mV. (**F**) The real-time current response of the dopamine sensor upon exposure to 1× PBS solution containing dopamine with different concentrations: 1 nM, 10 nM, 100 nM, 1 μM, 10 μM, and 100 μM. The current response is defined as $\Delta I_{ds}/I_0 \times 100\%$, where ΔI_{ds} and I_0 are the change of the source-drain current in the presence of the target and the initial current signal without the target, respectively. V_{ds} = 100 mV; V_G = 0 mV. (**G**) Selectivity of dopamine sensor. 5-HT: serotonin; DA: Dopamine; NE: Norepinephrine; GABA: Gamma-aminobutyric acid.

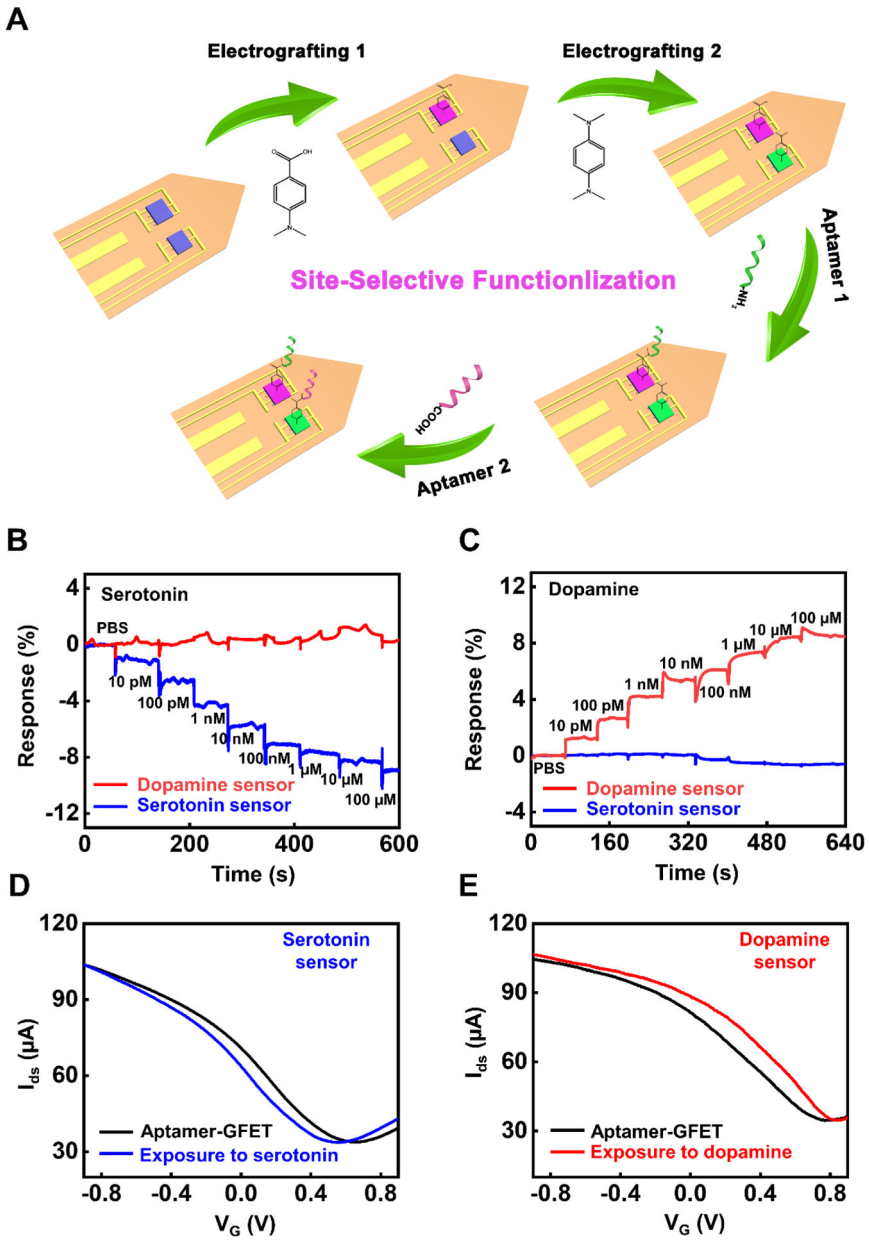

Fig. 4. Electrografting-enabled site-selective functionalization of G-FETs for multiplexed neurochemical monitoring in a single neural probe.

(**A**) Schematic illustration for the electrografting and functionalization process of G-FETs for multiplexed monitoring. The graphene surfaces of two G-FETs are sequentially functionalized with -COOH and -NH_2 groups through the electrografting method. After that, the serotonin aptamer with -NH_2 group and dopamine aptamer with -COOH group are immobilized on the graphene surfaces functionalized with -COOH and -NH_2, respectively. (**B**) Real-time response of serotonin and dopamine sensors when exposing a multiplexed neural probe to various serotonin concentrations ranging from 10 pM to 100 μM in 1× PBS. V_{ds} = 100 mV; V_G = 0 mV. (**C**) Real-time response of dopamine and serotonin sensors when exposing a multiplexed neural probe to various dopamine concentrations ranging from 10 pM to 100 μM in 1× PBS. V_{ds} = 100 mV; V_G = 0 mV. (**D**) Transfer curves of G-FET

serotonin sensor before and after introducing the target serotonin solution (100 μM in 1× PBS). V_{ds} = 200 mV. (**E**) Transfer curves of G-FET dopamine sensor before and after introducing the target dopamine solution (100 μM in 1× PBS). V_{ds} = 200 mV.

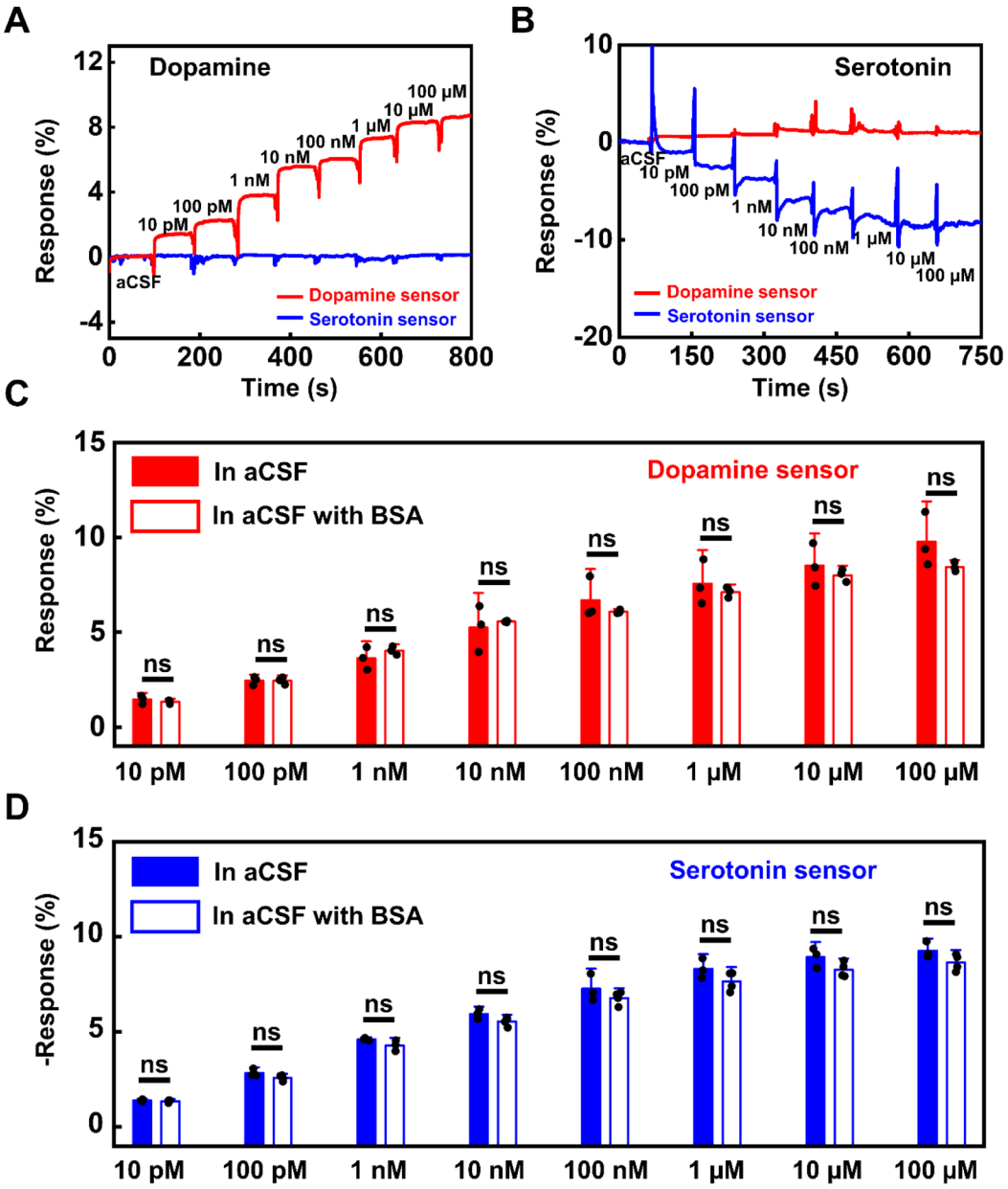

Fig. 5. Multiplexed neurochemical monitoring in aCSF with BSA protein.

Real-time response of the multiplexed neural probes when exposed to various concentrations of (**A**) dopamine and (**B**) serotonin solutions ranging from 10 pM to 100 μM in aCSF with 1 mg/mL BSA protein. V_{ds} = 100 mV; V_G = 0 mV Comparison of the electrical response of the multiplexed neural probes for monitoring (**C**) dopamine and (**D**) serotonin detection with and without 1 mg/mL BSA protein. n ≥ 3. All data are represented as means ±SD. The statistical significance of differences between mean values was determined using Student's t-tests for two independent means with one-tailed hypothesis. ns indicates that the difference of the means is not significant at the 0.05 level.

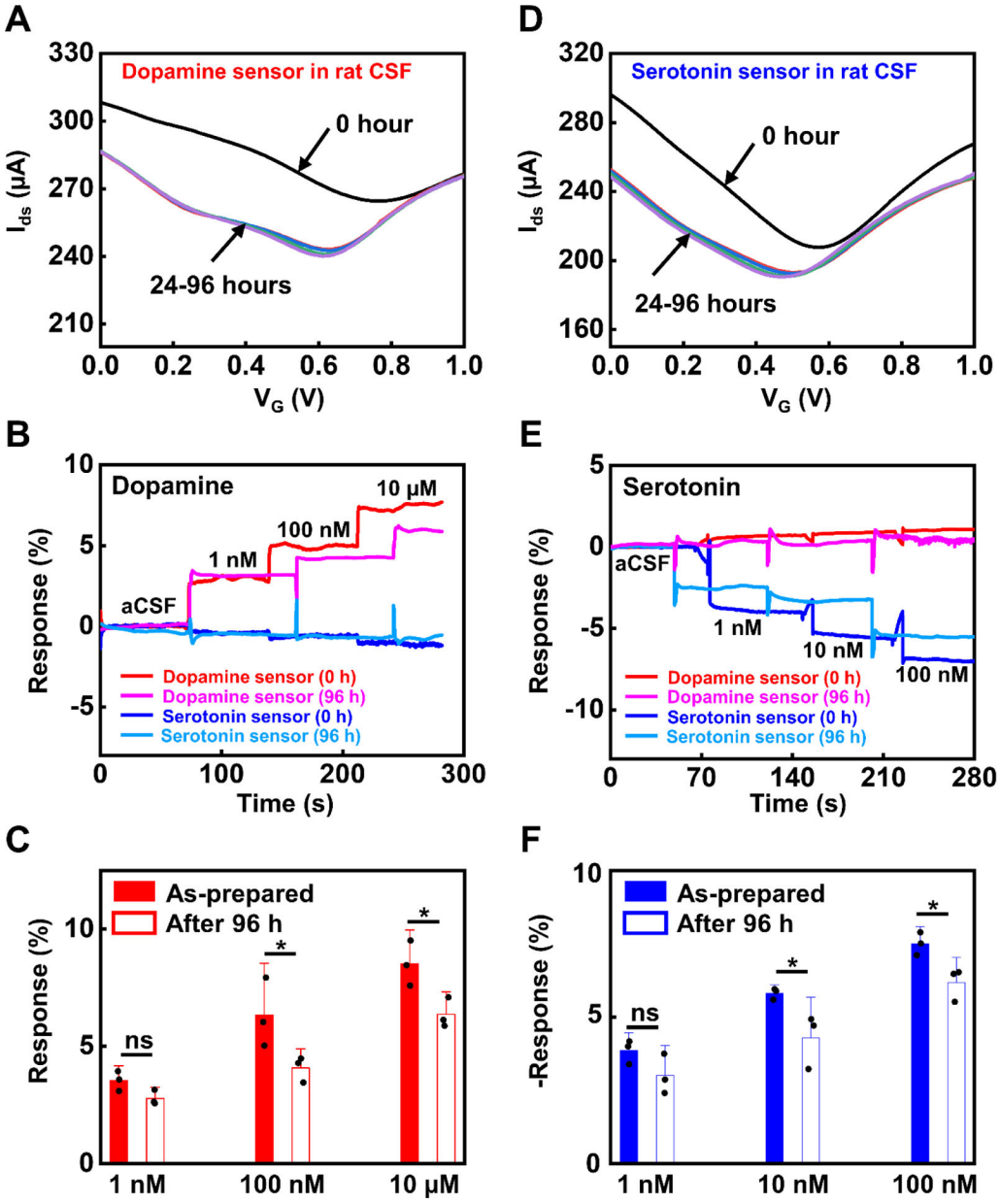

Fig. 6. Stability of multiplexed neural probes in rat CSF.

(**A**) Transfer curves of dopamine sensors before and after incubating in rat CSF for 24, 48, 72, and 96 hours at room temperature. V_{ds} = 200 mV. (**B**) Real-time responses of the multiplexed neural probes to various concentrations of dopamine in aCSF before and after incubating in rat CSF solution for 96 hours at room temperature. V_{ds} = 100 mV; V_G = 0 mV. (**C**) Comparison of the sensor response for monitoring dopamine before and after incubating in rat CSF solution at room temperature for 96 hours. (**D**) Transfer curves of serotonins sensors before and after incubating in rat CSF for 24, 48, 72, and 96 hours at room temperature. V_{ds} = 200 mV. (**E**) Real-time responses of the multiplexed neural probes to various concentrations of serotonin in aCSF before and after incubating in rat CSF solution for 96 hours at room temperature. V_{ds} = 100 mV; V_G = 0 mV. (**F**) Comparison of the sensor

response for monitoring serotonin before and after the incubation in rat CSF solution for 96 hours at room temperature. For C and F, n = 3, $*P < 0.05$. All data are represented as means ±SD. The statistical significance of differences between mean values was determined using Student's t tests for two independent means with one-tailed hypothesis. ns indicates that the difference of the means is not significant at the 0.05 level.

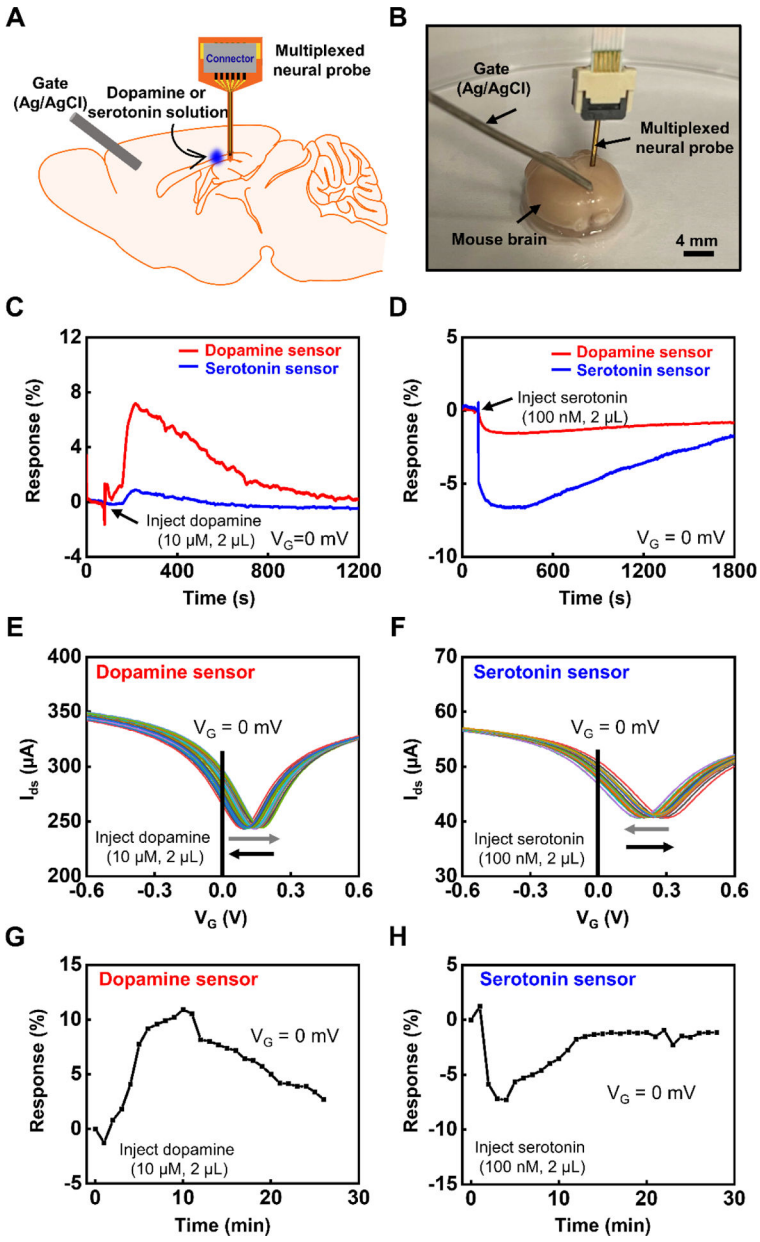

Fig. 7. ***Ex vivo*** **studies in harvested mice brain tissue.**

(**A**) Schematic illustration and (**B**) optical image of a multiplexed neural probe implanted into a harvested mouse brain tissue for monitoring dopamine and serotonin. Real-time response of a multiplexed neural probe implanted in the harvested mouse brain tissue upon the injection of (**C**) dopamine solution (10 μM in aCSF, 2 μL) and (**D**) serotonin solution (100 nM in aCSF, 2 μL). V_{ds} = 100 mV; V_G = 0 mV. Continuous monitoring of transfer curves of the neural probe implanted in the harvested mouse brain tissue when injecting (**E**) dopamine solution (10 μM in aCSF, 2 μL) and (**F**) serotonin solution (100 nM in aCSF, 2 μL). V_{ds} = 200 mV. Source-drain current response at V_G=0 mV for (**G**) dopamine and (**H**) serotonin sensor.